A validated co-simulation of grab and moist iron ore cargo
Replicating the cohesive and stress-history dependent behaviour of bulk solids

Mohajeri, M. Javad; de Kluijver, Wilbert; Helmons, Rudy L.J.; van Rhee, Cees; Schott, Dingena L.

DOI
10.1016/j.apt.2021.02.017

Publication date
2021

Document Version
Final published version

Published in
Advanced Powder Technology

Advanced Powder Technology 32 (2021) 1157–1169

Contents lists available at ScienceDirect

Advanced Powder Technology

journal homepage: www.elsevier.com/locate/apt

Original Research Paper

A validated co-simulation of grab and moist iron ore cargo: Replicating the cohesive and stress-history dependent behaviour of bulk solids

M. Javad Mohajeri [a,*], Wilbert de Kluijver [b], Rudy L.J. Helmons [a], Cees van Rhee [a], Dingena L. Schott [a]

[a] Delft University of Technology, Department of Maritime and Transport Technology, 2628 CD Delft, the Netherlands
[b] Nemag, Zierikzee 4301 RC, the Netherlands

ARTICLE INFO

Article history:
Received 29 July 2020
Received in revised form 16 December 2020
Accepted 5 February 2021
Available online 20 February 2021

Keywords:
DEM
Cohesive materials
Iron ore
Grab
Validation

ABSTRACT

The traditional design approach of grabs and other bulk handling equipment consists of manufacturing and testing physical prototypes. A novel design approach is to use a co-simulation of MultiBody Dynamics (MBD) and Discrete Element Method (DEM), in which the virtual prototype of a new concept interacts with bulk solids. Therefore, this study develops and validates a full-scale co-simulation that models the grabbing process of cohesive and stress-history dependent iron ore. First, by executing in-situ measurements during the unloading of a vessel, grab-relevant bulk properties of the cargo, such as penetration resistance, are determined. Second, full-scale grabbing experiments are conducted in the cargo hold, which allows the process to be recorded in realistic operational conditions. Third, full-scale co-simulation is set up using the material model that has been calibrated based on an elasto-plastic adhesive contact model. Fourth, the co-simulation is validated by comparing its predictions to experimental data from various aspects, such as the force in cables and the torque in winches. The validated co-simulation proves that the stress-dependent behaviour of cohesive cargo as it interacts with the grab could be captured successfully. Valuable information such as a grab's kinematics and dynamics, as well as the porosity distribution of collected bulk solids, can be extracted from the simulation, supporting engineers to enhance the design and operation of equipment.

1. Introduction

Due to the high demand of iron ore around the globe, approximately 9000 voyages of Cape-size bulk carriers, with capacities up to 400 000 DWT, are required annually [1]. At destination ports, grabs are often used to unload vessels delivering iron ore, as well as other dry bulk solids like coal. Grabs should unload bulk solids efficiently and reliably to minimize the mooring time of vessels, thus minimizing the operation costs of bulk terminals.

The general model of the grabbing process of bulk cargo (i.e. iron ore) using cable-based grabs is shown in Fig. 1a. The crane operator controls the grab using cables that are connected to driving winches. In addition to the grab design itself, the dimensions of a ship's hold, the properties of bulk cargo, the crane operator, winches and cables are all contributing elements in the grabbing process. Thus, predicting the performance of new design concepts is still challenging as it requires consideration of the interaction between multiple contributing elements.

The traditional design approach of grabs consists of manufacturing and testing physical prototypes. A real-scale prototype is usually designed based on the engineering experience of manufacturers. Next, the performance of the prototype as it interacts with bulk solids is evaluated at bulk terminals, thus deciding whether the design meets expectations. This approach is known to be time- and cost-intensive as multiple prototypes are manufactured before finalizing the product [2].

A novel approach to design grabs is virtual prototyping in interaction with bulk solids [2–4]. Lommen et al. [5] have developed a real-scale co-simulation between grabs and free-flowing iron ore material [6]. The co-simulation has been validated for simulating the grabbing process of iron ore pellets [7]. As shown in Fig. 1b, the co-simulation uses the framework developed by coupling two solvers, MultiBody Dynamics (MBD) and Discrete Element Method (DEM) [8]. The co-simulation requires a virtual crane operator, a CAD model of a grab, and a calibrated DEM material model as inputs.

In contrast to iron ore pellets, the majority of iron ore cargoes exhibit cohesive and stress-history dependent behaviour [6,9]. Cohesive forces between particles are created due to the liquid bridge, and hence the amount of moisture present influences mate-

* Corresponding author.
E-mail address: m.mohajeri-1@tudelft.nl (M.J. Mohajeri).

https://doi.org/10.1016/j.apt.2021.02.017

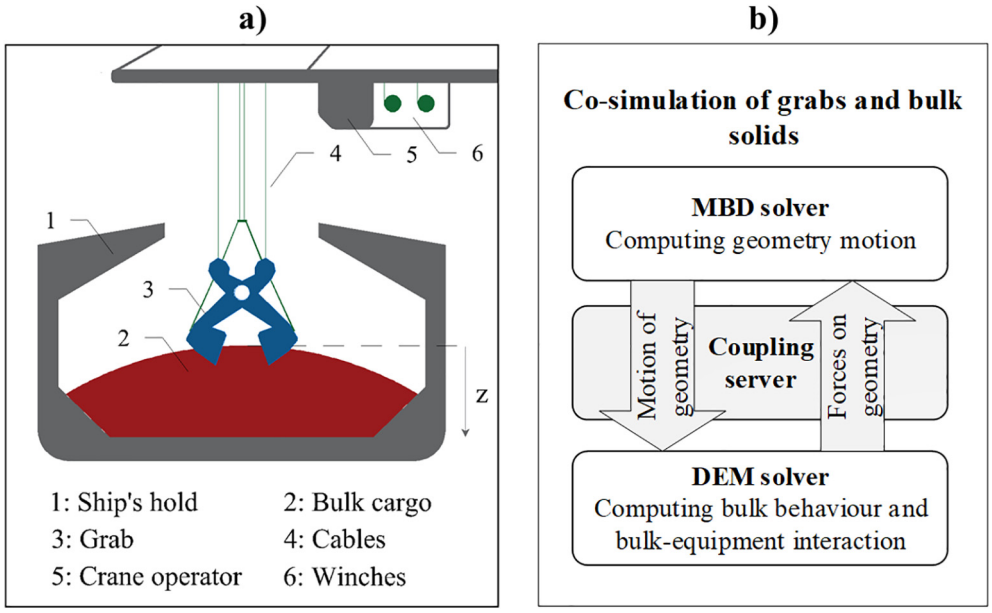

Fig. 1. (a) General model of the grabbing process (i.e. of iron ore) during unloading bulk carriers, (b) the co-simulation framework of grabs and bulk solid materials based on [8].

rial behaviour and its interaction with equipment. Furthermore, as the unloading starts and proceeds to greater depths, grabs touch the cohesive material that is pre-consolidated with a higher level of historical stress (pressure) [1]. A pre-consolidated situation means that the current vertical stress on bulk solids is less than the historical maximum stress. Consequently, during the unloading of a bulk carrier, the bulk responses of cohesive iron ore cargo, such as bulk density, shear strength, and bulk stiffness, are expected to vary over the cargo depth (z direction) [6]. The cohesive and stress-history dependent behaviours of bulk materials are not yet investigated in terms of interaction with grabs. Therefore, a test method first needs to be developed to determine the grab-relevant properties of cohesive bulk materials during the unloading of a cargo hold; second, a reliable DEM material model for cohesive bulk solids needs to be included in the co-simulation to enable the virtual prototyping of grabs.

In our previous work [10], DEM parameters were calibrated to simulate the cohesive and stress-history dependent behaviour of moist iron ore cargo with an elasto-plastic adhesive contact model. The common procedure to assure the validity of the model is to first calibrate with laboratory scale experiments [11,12] and next validate DEM simulations with industrial scale experiments [5,13–18]. Validation is achieved by comparing the results of the simulation and experiment, either in quantitative or qualitative ways [2,15,19–27]. To ensure design concepts can be evaluated under actual operational conditions, validating the model in full-scale is required [28,29].

Therefore, this study develops a validated co-simulation that models the grabbing process of moist iron ore cargo in full-scale industrial operations, by considering both cohesive and stress-history dependent behaviours in interaction with equipment. Fig. 2 displays the main steps required to develop the validated co-simulation of grabs and cohesive iron ore. In the first step, iron ore cargo is characterized during the unloading of a bulk carrier, as well as in the laboratory environment. The second step is to record the grabbing process under actual operational conditions, including the cargo depth as a variable, thus capturing the stress-history dependent behaviour of bulk material. The third step is to create a large-scale co-simulation of grabs and cohesive bulk solid cargo that has a practical computation time. The forth step is to validate that the co-simulation captures the grabbing process of the cargo accurately, considering essential outputs such as the static forces, dynamics, and kinematics of equipment. After validating the accuracy of the co-simulation, a comparative analysis is made on the grabbing process of two different types of bulk solids: cohesive and free-flowing iron ore products.

2. Bulk material characterization and validation method

This section describes the steps required to characterize bulk material and validate the co-simulation modelling of the grabbing process of cohesive iron ore cargo.

2.1. Characterizing bulk solid cargo

The bulk solid cargo is characterized in both laboratory and ship hold environments. The cargo is a sinter feed type of iron ore from the Carajas mines, which is one of the largest iron ore resources on earth [30]. The average density of the particles is 4500 kg/m^3 with a standard deviation of 125 kg/m^3. The median particle size, d_{50}, is equal to 0.88 mm.

The objective of in-situ measurements during unloading is to determine the properties of the cohesive iron ore cargo over its depth, z. The following bulk properties are relevant to the grabbing process [6], and are thus selected:

- Penetration resistance through initial penetration depth, $\Delta_{initial,S66}$
- Bulk density, ρ_b
- Moisture content, MC

Measuring penetration resistance and bulk density during the unloading process allows us to quantitatively investigate the level to which the cargo is densified over its depth. It is expected that moisture content also shows variation over cargo depth [31].

A test procedure is designed to determine the penetration resistance and bulk density using a single test device. Fig. 3 displays a schematic view of our designed test device, which is named *sam-*

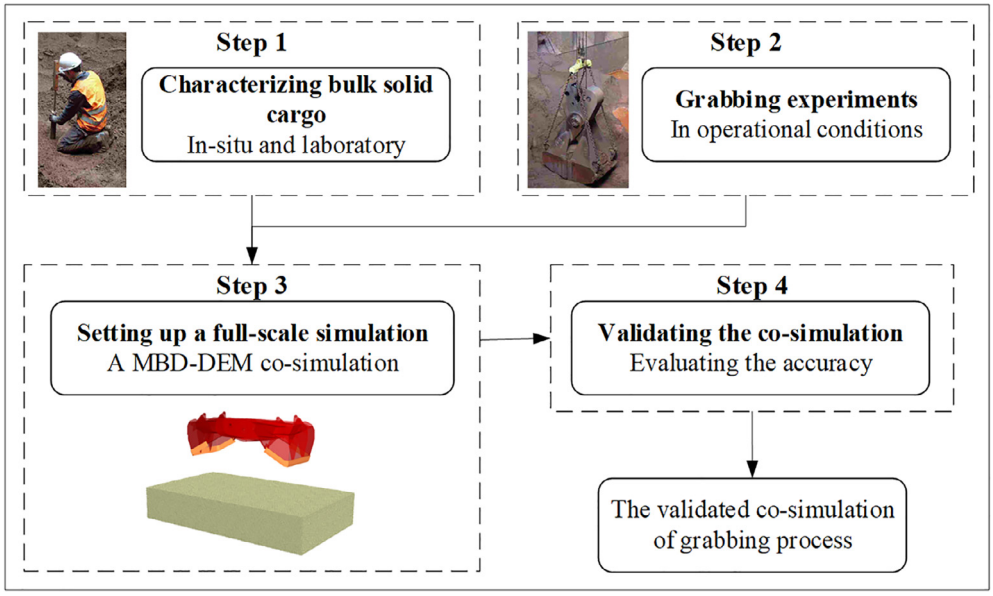

Fig. 2. Main steps to develop a validated co-simulation of grabbing process.

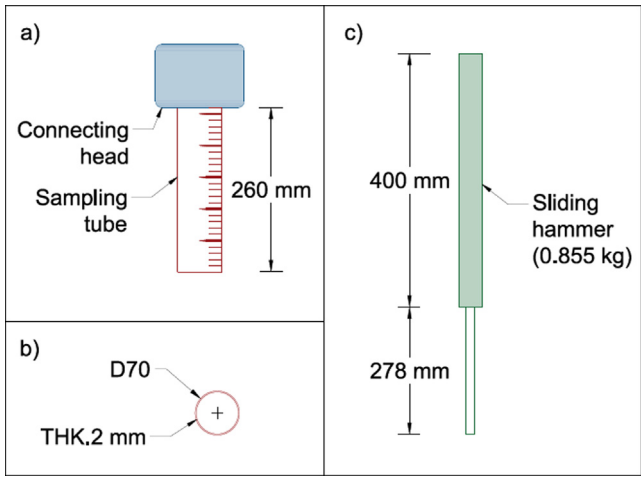

Fig. 3. Schematic view of sampling tube & sliding hammer (S66): a) sampling tube and connecting head to hammer, b) cross section view of the sampling tube, and c) the sliding hammer.

pling tube & sliding hammer (S66). It consists of two main components, a sampling tube (Fig. 3a and b) and a sliding hammer (Fig. 3c). The effective length of the sampling tube is 260 mm, with an inner diameter of 66 mm, and thickness of 2 mm. The hammer is 400 mm long with a mass of 0.855 kg, which is connected to a slide with a length of 278 mm. The sliding hammer can be fixed to the sampling tube using a connecting head.

Penetration resistance is determined based on a modified version of the *Standard Penetration Test* (ISO 22476–3). The tube is driven into the bulk surface with five consecutive drops of the sliding hammer, and next, the initial penetration depth of tube ($\Delta_{initial,S66}$) is recorded. The number of hammer drops is sufficient, as more hammer drops may result in a penetration depth greater than the effective length of the sampling tube.

The test continues by driving the sampling tube further into the bulk surface until the final penetration depth is reached. Next, the tube is carefully extracted to weigh the collected bulk solid specimen. It is ensured that the tube is extracted without losing the bulk specimen. Bulk density, ρ_b, is determined by Eq. (1).

$$\rho_b = \frac{M_s}{A_e.L_s} \tag{1}$$

where M_s is the weight of the collected specimen. L_s is the final penetration depth of the sampling tube that is determined by using the ruler, as shown in Fig. 3a. A_e is the inner cross-sectional area of the tube. The moisture content of samples is also measured in the laboratory using a drying oven, according to the method described in [32].

During the unloading process of bulk carriers, the bulk responses of fine moist iron ore ($\Delta_{initial,S66}$, ρ_b and MC) are expected to vary, as shown by the trends in Fig. 4. This hypothesis is based on field measurements [33], including the Cone Penetration Test (ASTM D3441), and moisture content over cargo depth, *z*, prior to commencing the unloading process.

Firstly, due to the void between particles, moisture is expected to transfer to greater depths during the voyage of bulk carriers. This results in the accumulation of moisture near the bottom of cargo holds [31]. Secondly, due to increasing vertical confining pressure over the cargo depth, lower initial penetration depth and higher bulk density values are respectively expected to occur by increasing *z* [6]. However, a saturated condition usually occurs

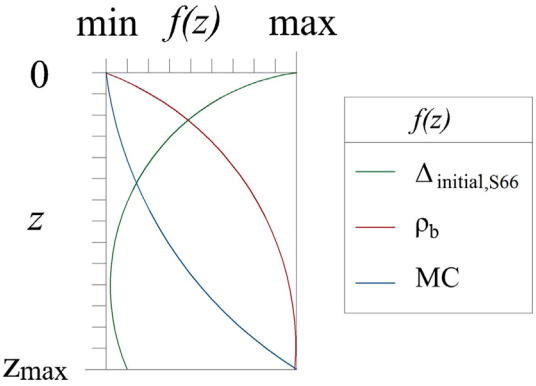

Fig. 4. Expected distribution of grab relevant bulk properties over cargo depth (*z*).

Table 1
Verifying the accuracy of the sampling tool (S66) in determining bulk density.

Measurement method	Rep	Average ρ_b	SD	SD [%]
ISO 17,828	5	1774	20	1.1
S66	10	1780	40	2.2

at the "wet bottom" of iron ore carriers [34], usually for $z/z_{max} \geq 0.8$.

2.1.1. Verifying the accuracy of the sampling tool (S66)

We verify whether the S66 device is accurate in determining bulk density of the cohesive iron ore sample. For this purpose, two different test methods, ISO 17828 [35] and S66, are used in the laboratory environment. In ISO 17828, bulk density is determined by using a rigid cylinder with the inner volume of 5 L. The bulk density results, including both average and standard deviation values, are compared in Table 1. Bulk density measurements using ISO 17828 are repeated five times, resulting in an average bulk density of 1774 kg/m^3 with an acceptable standard deviation of 20 kg/m^3. Measurements using the S66 device result in an average ρ_b of 1780 kg/m^3 with a standard deviation of 40 kg/m^3 in ten test repetitions.

Comparable average bulk density values can be measured using ISO 17828 and S66, with a minor difference in standard deviation values. Therefore, the accuracy of S66 in determining bulk density of the cohesive iron ore sample is verified.

2.1.2. Measurement plan

One primary variable is considered in the measurement plan: cargo depth (z). Bulk cargo is characterized in the in-situ conditions from the top of the cargo pile, z = 0 m, until z/z_{max} = 0.85. As grabs unload the bulk carrier, greater depths (z > 0 m) can be accessed. At each cargo depth, the measurement is repeated between three to five times, ensuring test repeatability. Three different cargo holds are accessed during the in-situ measurements.

The cargo depth, z, is determined using a laser ruler (HILTI PD 40). When standing on the bulk cargo surface, the hold depth index is read using the laser ruler device. The device is only able to measure the distance to the depth index, but unable to measure the laser beam orientation. Thus, the distance to three different points are measured for each cargo depth, allowing us to determine z with a maximum error of 0.5 m.

It usually takes more than a day to unload an ocean-bound bulk carrier. Therefore, unloading continues over a "night shift". No data can be collected during this time, as the in-hold environment is unsuitable for taking such measurements during that period.

Table 2
Measured parameters during the grabbing experiments.

Stage	Measured parameter
All stages	Force in cables
	Torque in winches
	Kinematics of geometry
Suspension	Payload
	Average porosity of collected bulk solids
	In-grab bulk sampling

2.2. Grabbing experiments

Fig. 5 shows five stages of the grabbing process, as introduced in [7]. In this figure, the red arrows indicate the cable velocity direction. The grab is lowered onto the bulk surface (Fig. 5a), ending with a certain penetration depth as the grab digs into the material (Fig. 5b). This continues by closing the grab and collecting the bulk solid (Fig. 5c). Once the grab is almost filled with the bulk solid, the hoisting stage commences (Fig. 5d). During experiments, the grabbing process usually ends with the suspension stage (Fig. 5e), which allows us to conduct further measurements, such as weighing the grab and collected mass together.

Table 2 presents the list of parameters measured in grabbing experiments. Two different types of parameters are measured. The signal type parameters are the following: the force in cables, the torque in winches, and the kinematics of grab geometry. Scalar type parameters are also recorded, such as payload and average porosity.

- Force in cables: the grab is operated on four cables and the tensile forces in these cables are measured using load cells. The load cells are located adjacent to driving winches of the crane. These load cells as well as other sensors are calibrated by the terminal operator on a regular basis. The load cells measure force in cables with a frequency of 2 Hz. The payload of grab, M_{DWT} can be determined using Eq. (2).

$$M_{DWT} = M_t - M_e \tag{2}$$

  where M_t is the total force in cables once the grab is hoisted after collecting bulk solids, and M_e is the total force in cables before collecting bulk solids. In other words, M_e corresponds to the weight of an empty grab.

- Torque in winches: the torque in each winch is determined separately with a frequency of 100 Hz. The sensor converts the electrical current produced by the crane's engine to torque data. These sensors are calibrated by the terminal operator on a regular basis.

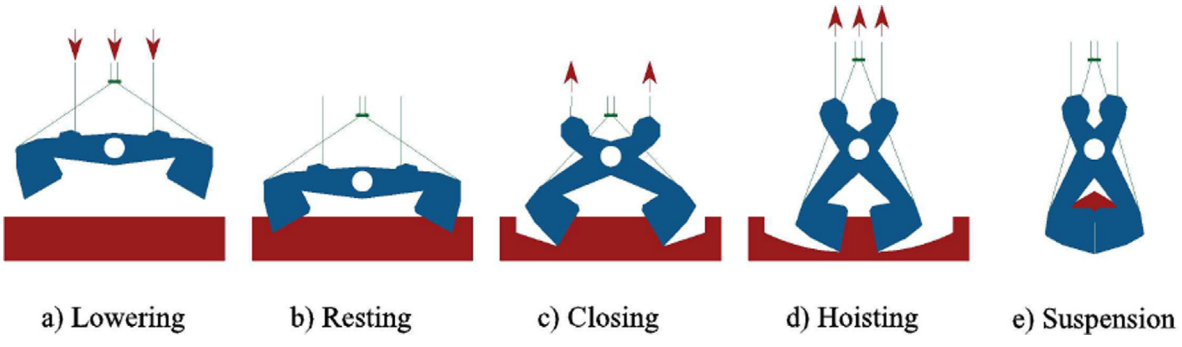

Fig. 5. The operation of the grabbing process consists of five stages: (a) Lowering onto the bulk surface, (b) Resting with slacked cables, (c) Closing by tensioning two cables, (d) Hoisting using all cables, and e) Suspending the grab if required.

- Kinematics of geometry: to record kinematics of the grab geometry, a video tracking technique similar to [7] is used. Basically, the grab geometry consists of two rigid bodies that revolves over a main hinge. For that reason, three markers are used that are sufficient to track the geometry movements in X-Z plane.
- Average porosity of collected bulk solids: once the grab is suspended, 3D-scanning technology is used to determine the volume of the collected bulk solids, V_{DWT}. First, point cloud images are taken using the Intel RealSense™ depth (SDK) camera. Second, a surface mesh is fitted on point cloud images, according to the method described in [36]. Fig. 6a shows an example of generated surface mesh, including the grab that contains collected bulk solids. Third, V_{DWT} is determined by importing the mesh surface of collected bulk solids into a 3D CAD model of the grab. The porosity of collected bulk solids, n_{DWT}, can then be calculated using Eq. (3).

$$n_{DWT} = 1 - \frac{M_{DWT}}{V_{DWT} \cdot \rho_s} \tag{3}$$

where ρ_s, particle solid density is equal to 4500 kg/m^3 [6].

- In-grab bulk sampling using S66-1000: once the grab is suspended, a sampling tube, *S66*, with the effective length of around 1 m is used to collect samples from the area highlighted in Fig. 6b. The tube is then carefully extracted from the bulk material. The sample is weighed, which allows for quantifying the porosity in a similar way compared to Eq. (3). The sampling using S66-1000 is repeated at least three times, ensuring the repeatability of the test.

2.2.1. Experimental plan

Two sets of experiments with different consolidation states are defined, of which multiple repetitions are performed.

- In the first experiment set, the process is recorded at the cargo depth of z = 7 m. The first experiment set includes: test 1.1, test 1.2 and test 1.3.
- In the second experiment set, the process is recorded at is z = 2.5 m. The second experiment set includes: test 2.1 and test 2.2.

The crane operator and bulk surface geometry are other possible influencing variables in our experiments. The velocity profile of closing and hoisting winches are recorded with a frequency of 100 Hz, thus a virtual crane operator can be modelled in the co-simulation, as shown in Fig. 1b. To minimize the influence of bulk surface geometry, grabbing experiments are executed on an adequately flat bulk surface.

2.3. A full-scale simulation setup

The co-simulation between MultiBody Dynamic (MBD) and DEM solvers uses the framework of [8], as shown schematically in Fig. 1b. The MBD simulation of the grab is set up using the real dimensions of the grab. In the virtual environment, the operation of the grab is simulated using a combination of winches, sheaves and cables [37].

A material model of the cohesive iron ore has been calibrated in part I of the current study [10]. The calibrated model is used in the current study to set up the DEM simulation. By applying the particle scaling rules of [38], a mean particle diameter of 55 mm is used in the simulation. The surface energy and constant pull-off force needs to be adjusted during the scaling of particles. Table 3 presents the main input parameters of the DEM simulation. For other DEM input parameters and the calibration procedure refer to [10].

To replicate a pre-consolidated condition in the simulation, DEM particles are compressed using a pressure-controlled plate. A quasi-static condition, as defined in [38], is maintained during compression. Once the desired pressure, is reached, the pressure-controlled plate is moved upward. Thus, a pre-consolidation condition is replicated in the DEM simulation.

Fig. 7 displays the DEM simulation environment, including the grab's geometry components. The dimensions of the material bed are selected after running a sensitivity analysis so that the grabbing process is not influenced by the boundaries. The in-situ measured winch velocity history is used as input in the co-simulation to replicate the grabbing process. In addition, modelling the actual distance between the grab and the trolley system of the crane could complicate the simulation setup unnecessarily. Thus, only the vertical position of the main hinge is analysed, as in the MBD simulation where the grab is positioned in the similar x-y coordinates compared to the winches.

To set up a full-scale DEM simulation of the grabbing process, the grab's components are separated into buckets and knives, as suggested by Lommen et al. [5]. The reaction forces from DEM particles on the bucket part is independent of particle size, thus the particle scaling rules of [38] can be applied. The penetration resistance against knives depends on the particle size [5], thus $\mu_{s,p\text{-}w}$ is adjusted to 0.2 for the interaction between knives and particles.

The DEM simulation of the grabbing process is run on a combination of CPU and GPU. This allows for reducing the computation time of a DEM-MBD co-simulation by around 6 times, compared to a CPU-based co-simulation. NVIDIA Quadro GP100 is used as

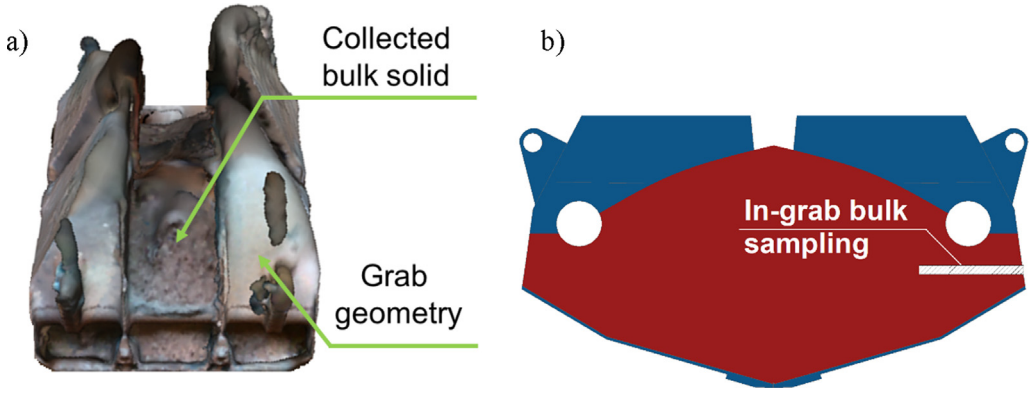

Fig. 6. (a) Generated 3D surface mesh, including grab geometry and collected bulk solid, (b) schematic cross-sectional view of grab and collected bulk solid, indicating the in-grab sampling area.

Table 3
Main input parameters of DEM simulation.

Parameter	Symbol	Unit	Value
Particle density	ρ_p	kg/m^3	4500
Particle diameter	d_p	mm	55
Particle shear modulus	G	MPa	7.5
Particle shape	Ψ_p	–	Single sphere
Normal and tangential contact modules, particle–particle	$f_{N,p\text{-}p}$ and $f_{T,p\text{-}p}$	–	EEPA [39]
Normal and tangential contact modules, particle-geometry	$f_{N,p\text{-}p}$ and $f_{T,p\text{-}w}$	–	Herz-Mindlin (no-slip)
Rolling contact module	f_R	–	Rotation restricted
Coefficient of static friction, particle–particle	$\mu_{s,p\text{-}p}$	–	0.31
Coefficient of static friction, particle-geometry	$\mu_{s,p\text{-}w}$	–	0.37
Constant pull-off force	$-f_0$	N	−0.2
Surface energy	$\Delta\gamma$	J/m^2	100
Plasticity ratio	λ_p	–	0.2

the graphics card in this study. Additionally, the scaling rules resulted in a reduction of 103 h for around 8 million particles to the computation time of around 4 h for 600 000 particles in the grabbing process of cohesive ore.

2.4. Evaluating accuracy of the co-simulation

For scalar type parameters (e.g. payload, average porosity), the mean of absolute relative differences is used to quantify error in the co-simulation. If y and y' represent measured scalar parameters in the experiment and the co-simulation, respectively, then $|e|_{mean}$ is determined according to Eq. (4) for a number of test repetitions. In the current study, an $|e|_{mean} \leq 10\%$ is considered an acceptable outcome for validating the accuracy of the co-simulation.

$$|e|_{mean} = \sum_{k=1}^{N_e} 100 \left| \frac{y_k - y'_k}{y_k} \right| \tag{4}$$

Signal type parameters (e.g. force in cables, torque in winches) are compared between the experiments and simulations using the coefficient of determination, R^2, as described by Weisberg [40]. To validate the force in cables and the torque in winches, Lommen et al. [7] suggested that minimum R^2 values of 0.9 and 0.8 are required respectively.

3. Results

In this section, the results of in-situ bulk cargo characterization, as well as the validation of the DEM-MBD model, are presented.

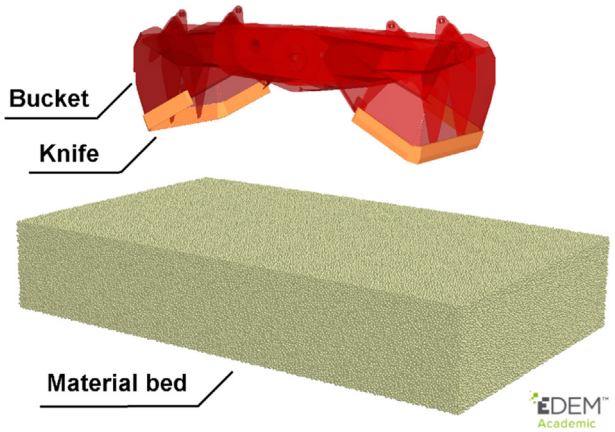

Fig. 7. Main components in the DEM simulation, including material bed, the grab's buckets, and the grab's knives.

3.1. Bulk cargo characterization during unloading

Fig. 8 presents the outcome of the in-situ measurements on bulk properties over cargo depth, including initial penetration depth (Fig. 8a), bulk density (Fig. 8b), and level of moisture content (Fig. 8c). The purple-coloured area indicates the "night shift" period in which no data was measured.

According to Fig. 8a, $\Delta_{initial,S66}$ in the first 2.5 m of the cargo depth is>75 mm in all three measurements; while in other data points, when $z \geq 6$ m, the initial penetration depth of S66 is smaller than 75 mm. A higher deviation in results is observed when $z \leq 2.5$ m, compared to when $z \geq 6$ m. However, a clear trend is that $\Delta_{initial,S66}$ in the later situation ($z \geq 6$ m) is always smaller than in the former ($z \leq 2.5$ m). Some level of increase in $\Delta_{initial,S66}$ is observed when $z \geq 8$ m, compared to $8 > z \geq 6$, which is probably due the correlation between the penetration resistance of material and its moisture content.

According to Fig. 8b, bulk density values in the first 2.5 m of the cargo depth is lower than 2400 kg/m^3, and the bulk density of three out of four data points shows comparable values to our laboratory measurements (Table 1). In contrast, at greater depths ($z \geq 6$ m), the bulk density of the cohesive iron ore cargo increases significantly (up to around 3100 kg/m^3).

According to Fig. 8c, the moisture content is between 8.4% and 9% when $z \leq 6$ m, while it increases up to 10% when $z > 6$ m. In general, due to the void between particles, moisture transfers to greater depths during the voyage of bulk carriers. Similarly, a non-linear increase in moisture content has been observed for other iron ore cargoes [33]. The average moisture content of the cargo is 9.1%, with a standard deviation of 0.5%.

In conclusion, an increasing densification of the cohesive iron ore over the cargo depth is observed, which is in line with the expected trends shown in Fig. 4. This has been supported by the considerable changes of $\Delta_{initial,S66}$ and bulk density values over cargo depth that have been determined during the unloading of the vessel. Thus, during the lowering stage, grabs penetrate into increasingly pre-consolidated bulk solids. To model the grabbing process of cohesive bulk solids in a realistic way, the increasing levels of pre-consolidation over the cargo depth needs to be replicated in the DEM simulation setup.

3.2. Validating the co-simulation

Two sets of grabbing experiments are conducted where the dry-based moisture content is 8.8 ± 0.2%. The DEM material model is calibrated based on the moisture content of 8.7%, which is expected to replicate cargo conditions properly. Grabbing experiments are conducted at two different cargo depths, which correspond to z equal to 7 and 2.5 m. Due to cargo weight, the overburden pressure creates a pre-consolidated condition at men-

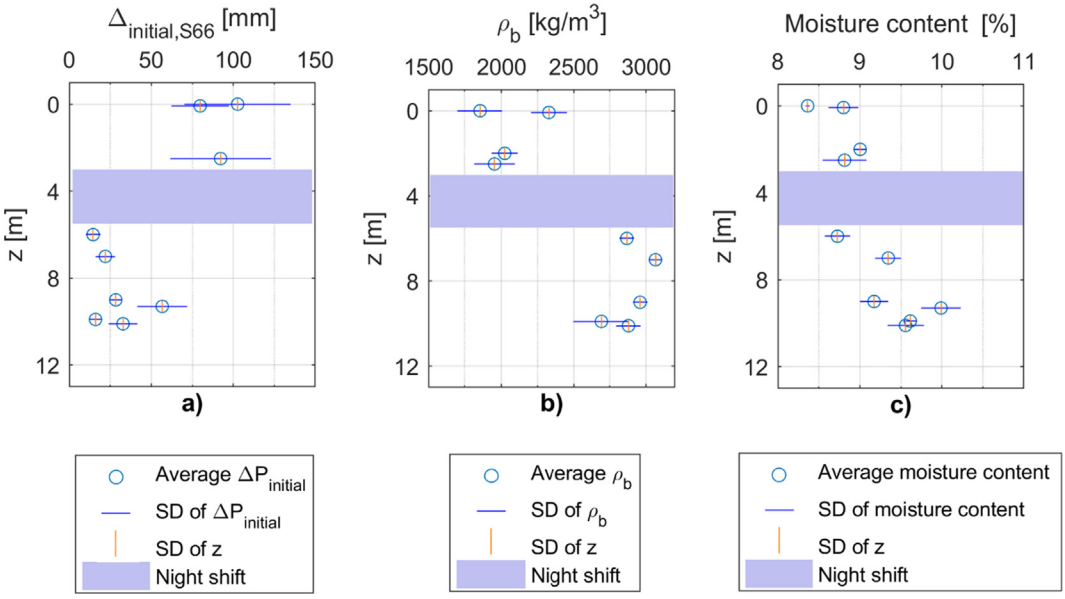

Fig. 8. Grab-relevant properties of cohesive iron ore over cargo depth: (a) initial penetration depth, (b) bulk density, and (c) level of moisture content.

tioned cargo depths [1]. The overburden pressure, σ_{pre}, can be approximated by multiplying cargo depth and average cargo density together; the average cargo density is 2800 kg/m^3. For example, in the experiment set 1, corresponding to z = 7 m, the historical pressure is equal to approximately 200 kPa. Fig. 9 compares the bulk density in simulated pre-consolidated conditions with experimental results of [6] on the same iron ore sample. Bulk density values at σ_{pre} equal to 65 and 200 kPa are adequately replicated in the DEM simulations.

Fig. 10 shows the simulated grabbing process during four different stages of the operation: a) Lowering, b) Rest, c) Closing, and d) Hoisting. The suspension stage is not included in that simulation.

3.2.1. Experiment set 1: Cargo depth of 7 m

The experimental results of the grabbing process are compared with predictions of the DEM-MBD co-simulation. Table 4 compares the payload in the experiments, $M_{DWT,exp}$, when the cargo depth is 7 m, to the simulated payload values, $M_{DWT,sim}$. The corresponding pre-consolidated situation is simulated by applying a uniform pressure of 200 kPa on the bulk surface prior to the grabbing process.

In the experiment set 1, an average $M_{DWT,exp}$ = 26.1 ton is determined with a standard deviation of 1.2 ton. The co-simulation replicates the payload values, with an average $M_{DWT,sim}$ = 25.7, with a standard deviation of 1.2 ton. The difference between simulated payloads and experimental results, $|e|_{mean}$, is 1.8%, with the maximum value of |e| = 5.8%. The small error is probably caused by idealizing the bulk surface in the simulation and its operational characteristics. Also, Schott et al. [7] have validated the simulation of the grabbing process of free-flowing iron ore products with values of $|e| \leq 6.0\%$. Therefore, the payload values for test 1 are simulated adequately, compared to reality.

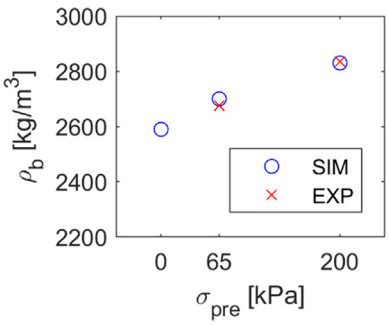

Fig. 9. The DEM simulation setup adequately replicates the bulk density in pre-consolidation situations.

Test 1.1 is selected for further analysis in terms of the force in cables and the torque in winches. Fig. 11 compares the total force in cables between the experiment and the co-simulation. The total force during the lowering stage (L) represents the empty weight of grab, M_e. Once the grab is resting on the bulk solid, cables go slack, thus, the total force drops. By tensing the closing cables during the next stage (C), the grab starts to collect the bulk solid. This continues by involving the hoisting cables and eventually lifting the grab out of the bulk solid. In test 1.1, the crane operator moves the grab toward the quay side, and therefore, no suspension stage (S) is present. The force over all stages is predicted accurately with an overall coefficient of determination of 0.959.

To validate the grab's dynamics, the torque of the closing and hoisting winches during a grabbing cycle are compared in Fig. 12. Similar to the force data (Fig. 11), the torque in the closing and hoisting winches are adequately predicted. Only during the hoisting stage (H) does the torque start to deviate slightly from the experimental data, for both closing (Fig. 12a) and hosting (Fig. 12b) winches. The predicted closing and hoisting winches have the coefficient of determination values of 0.947 and 0.934 respectively, for the entire time span. Therefore, the results confirm the grab's dynamics in test 1 are correctly predicted in the co-simulation.

Fig. 13 displays the three markers that we use to track the movements of the geometry during the grabbing process. Left and right markers represent the movement of the left and right grab's buckets respectively. The hinge marker represents the main hinge of the geometry where the grab's two buckets revolve.

Fig. 14 compares the position of the markers between the simulation and the experiment. The position of the markers is analysed when the grab geometry is within reach of the video camera. In other words, the initial part of the lowering stage and the last five seconds of the hoisting stage are excluded from the analysis. These excluded areas are not of interest as the grab

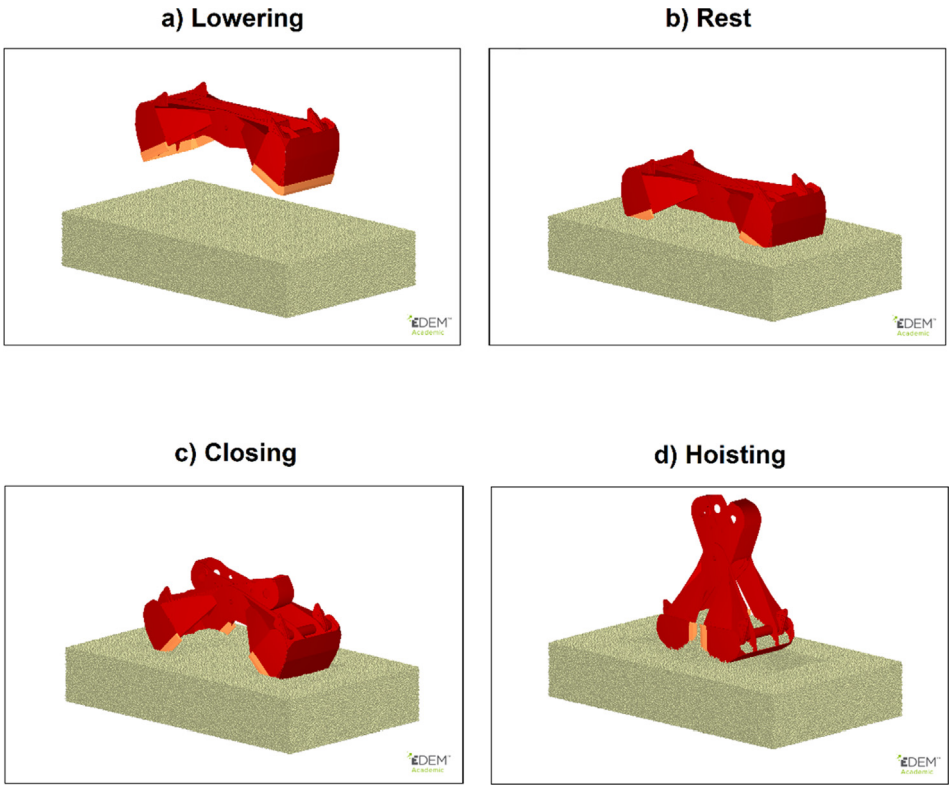

Fig. 10. The simulated grabbing process in different operation stages: (a) Lowering, (b) Rest, (c) Closing, and (d) Hoisting.

Table 4
Comparison between simulated payload and experimental measurements in test 1 (z = 7 m).

Test	$M_{DWT,exp}$ [ton]	$M_{DWT,sim}$ [ton]	|e| [%]
1.1	24.9	25.7	3.2
1.2	25.7	24.2	5.8
1.3	27.8	27.1	2.5
Mean	26.1	25.7	1.8

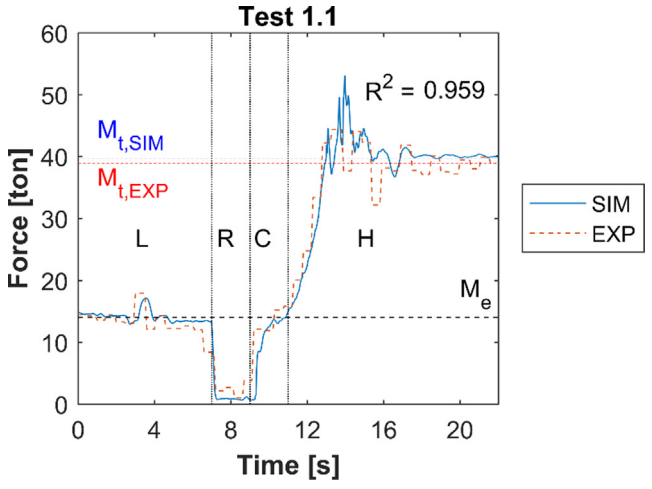

Fig. 11. Load comparison in test 1.1.; Grab operation consists of lowering of the grab (L), resting on the surface (R), closing (C) and hoisting (H).

mechanism is not operational (no closing or opening) and there is no dynamic interaction with material (lowering and hoisting).

For all markers, the desired coefficient of determination, $R^2 > 0.9$ is met with values exceeding 0.96. The observed comparisons in Fig. 14 confirm that the co-simulation is capable of predicting the grab's kinematics for a pre-consolidated cohesive bulk solid cargo.

With the aid of 3D-scanning technology, the volume of collected bulk solids, V_{DWT}, in the grab is determined for test 1.3, and the average porosity, n_{DWT}, is calculated using Eq. (3). Fig. 15a presents how porosity is distributed in the simulation. The densification is at its lowest level near the free surface of bulk material, while due to existing compression forces, the material becomes more densified in its central region. The self-weight of bulk material, as well as the force applied by the grab geometry, are the acting compressive forces. A sampling tube, *S66*, is penetrated 0.60 m into the grabbed material and used to collect samples in the region highlighted in Fig. 15b. The sampling is repeated three times, resulting in the porosity of 0.468 for the highlighted region. The simulated porosity for the same region is 0.480, indicating that simulated porosity distribution replicates reality accurately with |e| = 2.5%. Table 5 presents the comparison of M_{DWT} and n_{DWT}. The payload is replicated with a 2.5% difference between the simulation and the experiment. V_{DWT} is predicted accurately with |e| = 1%; this results in an adequate prediction of the average porosity with |e| = 5.8%.

3.2.2. Experiment set 2: Cargo depth of 2.5 m

Table 6 compares the payload in experiments, $M_{DWT,exp}$, with the simulated payload, $M_{DWT,sim}$, when the cargo depth is 2.5 m. The corresponding pre-consolidated situation is created by applying a uniform pressure of 65 kPa on the bulk surface proceeding the grabbing process.

In the experiment set 2, an average $M_{DWT,exp}$ = 26.4 ton is determined with a standard deviation of 0.3 ton. The co-simulation replicates payload values accurately, with an average

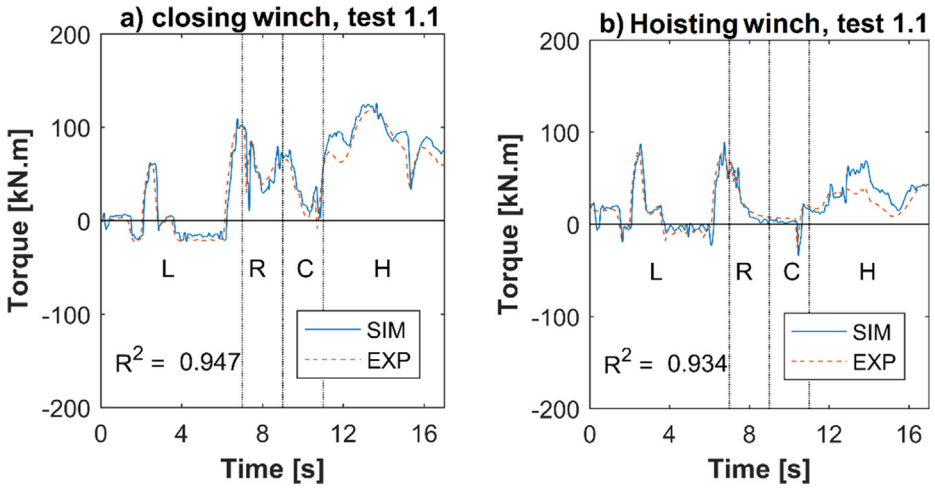

Fig. 12. Torque comparison in test 1.1., (a) closing winch, (b) hoisting winch; Grab operation consists of lowering of the grab (L), resting on the surface (R), closing (C) and hoisting (H).

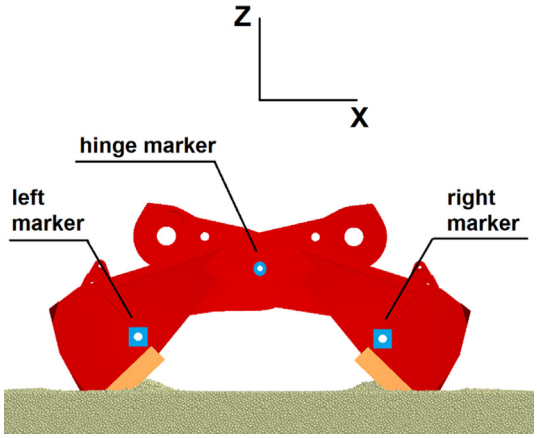

Fig. 13. Three markers are used to quantify kinematics of the grab.

$M_{DWT,sim}$ = 26.3 with a standard deviation of 0.7 ton. Negligible differences between simulated payloads and experimental results are observed with $|e|_{mean}$ = 0.4%.

In addition, test 2.2 is selected to further validate the adequacy of the co-simulation. Fig. 16 compares the total force in cables between the experiment and the co-simulation. The cables do not go fully slack during the rest stage (R), and therefore, the total force does not drop to zero. All four stages are replicated accurately in the co-simulation with R^2 = 0.957, confirming that the desired accuracy is also met when the cargo depth is 2.5 m.

The volume of collected bulk solids, V_{DWT}, in the grab is determined for test 2.2 using the 3D-scan technology, and the average porosity, n_{DWT}, is calculated using Eq. (3). Table 7 presents the comparison of M_{DWT} and n_{DWT}. The payload is replicated with a 1.1% relative difference between the simulation and the experiment. V_{DWT} is predicted with |e| = 5.3%; this results in an adequate prediction of the average porosity with the absolute different of 0.029 and |e| = 8.8%. The sampling tube, *S66*, is penetrated 0.60 m into the grabbed material and used to collect samples in the region highlighted in Fig. 17. The sampling is repeated three times, resulting in the porosity of 0.410 ± 0.020 for the highlighted region. The simulated porosity for the same region is 0.440 ± 0.010, indicating that simulated porosity distribution replicates reality adequately with the absolute difference of 0.030 and |e| = 8.6%.

The grabbing process in two levels of pre-consolidation, corresponding to 65 kPa and 200 kPa, are validated. This confirms that the co-simulation is capable of capturing the grabbing processing of cohesive and stress-history dependent iron ore cargo. Further analysis on the grabbing process can help in gaining insight into the grabbing process of cohesive bulk solids.

4. Discussion of stress-history dependency

In the previous section, we showed that the co-simulation can replicate a realistic grabbing process of cohesive iron ore, including two different levels of pre-consolidation. To further quantify the influence of pre-consolidation, additional simulations are carried out as shown in Table 8. The grabbing process of the cohesive iron ore, Carajas SF, in five different levels of pre-consolidation, is compared with the same process for free-flowing cargo: iron ore pellets. Pre-consolidation does not play a role in the grabbing process of iron ore pellets; thus, it is a proper option for our comparative analysis on the effect of σ_{pre} on the grabbing process. The validated co-simulation of the grab with iron ore pellets is created in [7]. The grab dimensions and other inputs of the MBD simulation are kept as constants in the simulation plan, thus, the grabbing process can be investigated in comparable conditions. 300 kPa is selected as the highest pre-consolidation level, which is sufficient to create a pressure state existing at the cargo depth of around 11 to 14 m. Therefore, the grabbing process of cohesive and free-flowing iron ore products is compared for an operational range of cargo depths.

Fig. 18 compares the footprint when the grabbing process is finished, and the grab has been lifted out of the material bed. Fig. 18a shows the grab's footprint on the cohesive material bed. The cutting trajectory of the grab's knives can be seen clearly. In addition, the steep slope, which is clear at both sides, represents the initial penetration depth of the grab in resting state. A similar angle is observed during the grabbing process of cohesive iron ore in the cargo hold condition, allowing for the determination of the initial penetration of the grab, $\Delta_{grab,initial}$. At the cargo depth of around 7 m, an average $\Delta_{grab,initial}$ of 0.39 m, with a standard deviation of 0.05 m, is measured for the cohesive cargo.

Fig. 18b shows the grab's footprint on the free-flowing material bed. Due to relatively low slope stability, particles flow once the grab has cut the bulk material. This results in a disturbed footprint, where the cutting trajectory of the grab's knives is no longer visible.

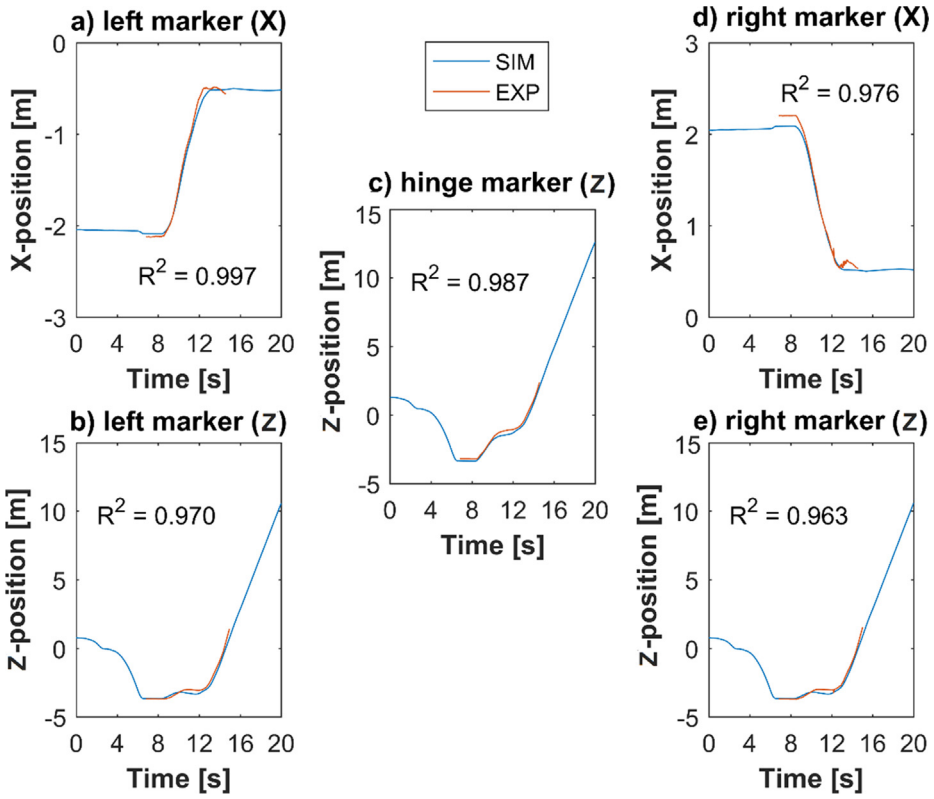

Fig. 14. Comparison between simulating and video-tracking of the three applied markers on the grab, on pre-consolidation of 200 kPa in test 1.1. (a) X-position of the marker on the left bucket, (b) Z-position of the marker on the left body, (c) Z-position of the marker on the main hinge, (d) X-position of the marker on the right bucket, and (e) Z-position of the marker on the right body.

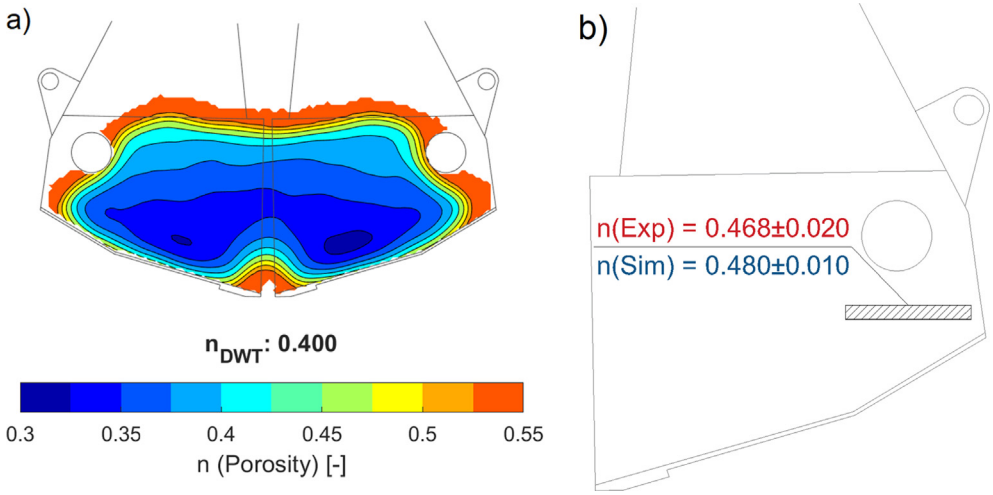

Fig. 15. (a) Simulated porosity distributon, and (b) porosity comparison between experiment and simulation.

Table 5
Validating volume and porosity of collected bulk solid for test 1.3.

Test 1.3	M_{DWT} [ton]	n_{DWT} [-]
Experiment	27.8	0.375
Simulation	27.1	0.400
|e| [%]	2.5	5.8

Table 6
Comparison between simulated payload and epxerimental measurements in test 2 (z = 2.5 m).

Test	$M_{DWT,exp}$ [ton]	$M_{DWT,sim}$ [ton]	|e| [%]
2.1	26.1	25.7	1.5
2.2	26.7	27.0	1.1
Mean	26.4	26.3	0.4

Fig. 19a displays the effect of pre-consolidation on the initial penetration of the grab into bulk material in a resting state. Pre-consolidation does not play a role in $\Delta_{grab,initial}$ for free-flowing cargo. For cohesive cargo, the initial penetration of the grab decreases from 0.67 m to 0.37 m by increasing the

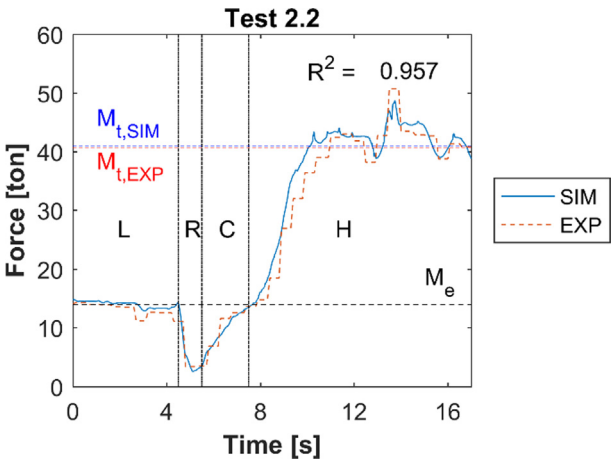

Fig. 16. Load comparison in test 2.2.; Grab operation consists of lowering of the grab (L), resting on the surface (R), closing (C) and hoisting (H).

Table 7
Validating volume and porosity of collected bulk solid for test 2.2.

Test 1.3	M_{DWT} [ton]	n_{DWT} [-]
Experiment	26.7	0.340
Simulation	27.0	0.369
|e| [%]	1.1	8.8

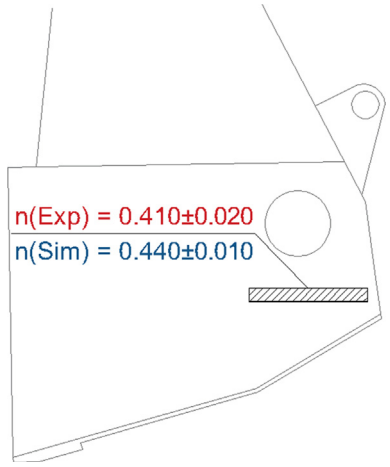

Fig. 17. Porosity comparison between experiment and simulation in Test 2.2.

Table 8
Variables in the investigation on the effect of pre-consolidation on the grabbing process.

Pre-consolidation levels [kPa]	[0 20 65 200 300]
Bulk materials	Carajas SF (cohesive iron ore) Pellets (free-flowing iron ore)

pre-consolidation level from 0 to 300 kPa. A comparable $\Delta_{grab,initial}$ is measured between the experiments and simulation for σ_{pre} = 200 kPa.

Fig. 19b displays the effect of pre-consolidation on the maximum cutting depth of the grab measured during the closing stage. $\Delta_{grab,max}$ is constant for free-flowing cargo, while it decreases considerably for cohesive cargo.

As shown in Fig. 19c, cohesive cargo densifies under the effect of pre-consolidation, which is the reason behind the stress-history

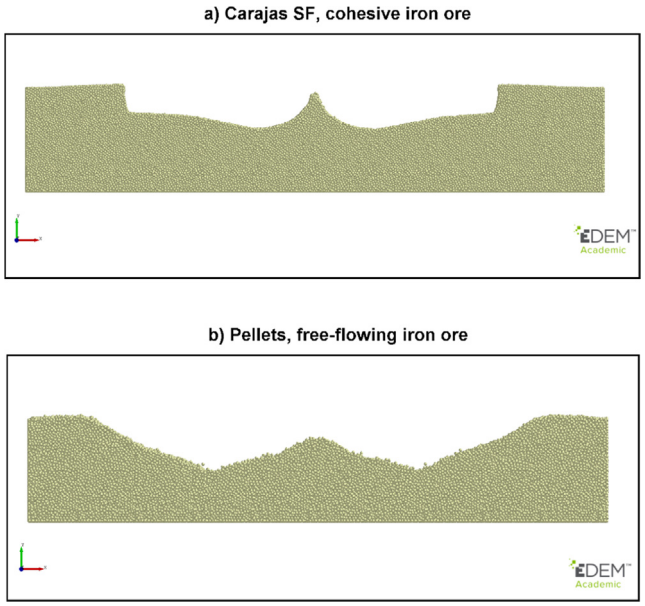

Fig. 18. Footprint of the grabbing process on two types of iron ore: (a) Carajas SF, and (b) Pellets.

dependent behaviour captured for $\Delta_{grab,initial}$ and $\Delta_{grab,max}$. As expected, the bulk density of free-flowing cargo is constant under the effect of pre-consolidation. Also, the bulk density of this free-flowing cargo is lower than the cohesive cargo, thus a higher grab payload is expected for Carajas SF.

The grab's payload under the effect of pre-consolidation is illustrated in Fig. 20. The payload, M_{DWT}, at 0 kPa pre-consolidation is considerably larger for cohesive material compared to the free-flowing material. Bulk density and maximum cutting depth are the reasons behind such a difference. The stress-history dependent behaviour of the cohesive cargo results in a negative correlation between M_{DWT} and σ_{pre}, while a constant payload is captured for the free-flowing cargo.

5. Conclusion

This paper successfully developed a validated co-simulation to accurately simulate the grabbing process of cohesive and stress-history dependent iron ore. Conducting full-scale grabbing experiments in the cargo hold allowed the process to be recorded under realistic operational conditions. The predictions of the co-simulation compared well to experimental data in all aspects, including force in cables, torque in winches, kinematics of geometry, payload, collected volume and average porosity of bulk solid. The same validation procedure can be applied to simulate the grabbing process of other materials, such as coal and grains.

In-situ measurements of bulk density and penetration resistance, using the developed test method (S66), quantified an increasing densification over the cargo depth. The co-simulation was validated for two different levels of cargo depth to ensure capturing the stress dependent behaviour of the bulk material.

A negative correlation between pre-consolidation level and payload was observed. Multiple grab-relevant factors are affected when a pre-consolidation situation is created for cohesive materials; the increasing density of bulk material results in a lower penetration/cutting depth of grab, both at rest and closing stages.

Co-simulation setups allow for analysing the design performance of both free-flowing and cohesive iron ore under the effect of consolidation. Valuable information, such as the cutting trajectory, porosity distribution, and the volume of collected bulk solids

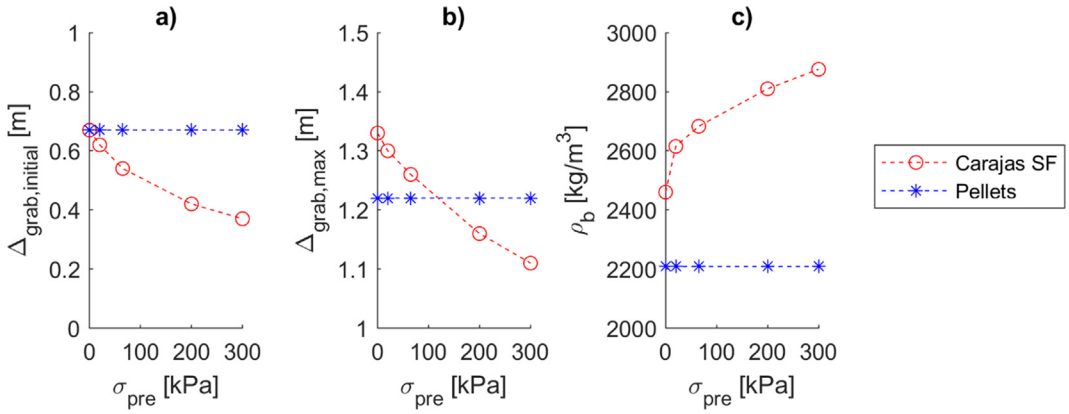

Fig. 19. Effect of pre-consolidation on: (a) the initial penetration depth of grab, (b) the maximum cutting depth of grab, and (c) the bulk density of cargo prior to the grabbing process.

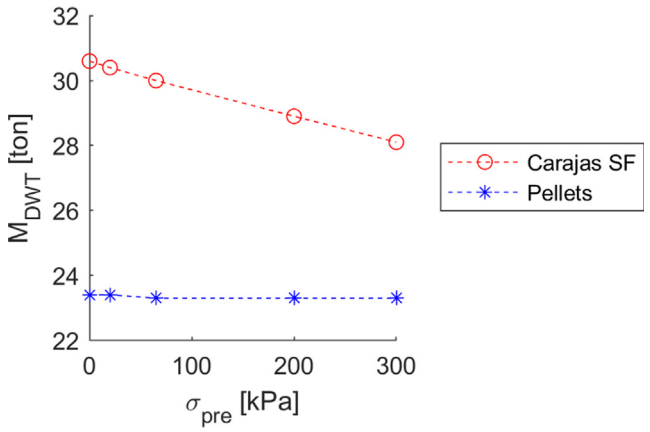

Fig. 20. Direct effect of pre-consolidation on the grab payload for cohesive and free-flowing iron ore cargoes.

can be extracted from the simulation. This can support designers and engineers in gaining insight into and improving grab performance.

The developed co-simulation is beneficial not only for grab manufacturers, but for other stakeholders who are active in the grab industry, such as bulk handling terminal operators. The co-simulation enables the possibility of creating an automated operation system of grabs. Realistic operational conditions, such as variations of pre-consolidation level and bulk surface geometry, can be included in the simulation environment, thus creating the opportunity to test such an automated operation system.

Declaration of Competing Interest

The authors declare that they have no known competing financial interests or personal relationships that could have appeared to influence the work reported in this paper.

Acknowledgements

The authors would like to acknowledge the support of Harry Post and his colleagues from the Department of Raw Material Handling at TATA Steel, the Netherlands, for their contribution in conducting the in-situ experiments in the cargo hold environment. Also, the support of Adam Bezuijen from the Department of Civil Engineering at Ghent University, Belgium, in designing the in-situ test method is acknowledged.

References

[1] M. Mohajeri, F.M. Sickler, C. van Rhee, D.L. Schott, A consolidation-penetration test for wedge-shaped penetration tools, FME Trans. 46 (2018) 393.
[2] S.W. Lommen, Virtual prototyping of grabs: co-simulations of discrete element and rigid body models, Delft University of Technology, 2016.
[3] H. Otto, A. Zimmermann, M. Kleiber, A. Katterfeld, Optimization of an orange peel grab for wood chips, 2019.
[4] R.J. Kuiper, X. Chen, J.C.L. Frumau, S.A. Miedema, Reduction of Energy Consumption When Using a Grab for Deep-Sea Mining Operations, in: Offshore Technology Conference, Offshore Technology Conference, 2016.
[5] S. Lommen, M. Mohajeri, G. Lodewijks, D. Schott, DEM particle upscaling for large-scale bulk handling equipment and material interaction, Powder Technol. 352 (2019) 273–282, https://doi.org/10.1016/j.powtec.2019.04.034.
[6] M.J. Mohajeri, M. van den Bos, C. van Rhee, D.L. Schott, Bulk properties variability and interdependency determination for cohesive iron ore, Powder Technol. (2020).
[7] D.L. Schott, M.J. Mohajeri, J. Jovanova, S.W. Lommen, W. de Kluijver, Design framework for DEM-supported prototyping of grabs by industrial-scale validation, In Progress, 2020.
[8] S. Lommen, G. Lodewijks, D.L. Schott, Co-simulation framework of discrete element method and multibody dynamics models, Eng. Comput. (2018).
[9] J.P. Morrissey, Discrete Element Modelling of Iron Ore Pellets to Include the Effects of Moisture and Fines, The University of Edinburgh, 2013.
[10] M.J. Mohajeri, C. van Rhee, D.L. Schott, Replicating stress-history dependent behaviour of cohesive solid materials - part I: feasibility and definiteness in DEM calibration procedure, In Progress, 2020.
[11] M.J. Mohajeri, Do huy, D.L. Schott, DEM calibration of cohesive material in the ring shear test by applying a genetic algorithm framewrok, Adv. Powder Technol. 31 (2020) 1838–1850.
[12] F. Ye, C. Wheeler, B. Chen, J. Hu, K. Chen, W. Chen, Calibration and verification of DEM parameters for dynamic particle flow conditions using a backpropagation neural network, Adv. Powder Technol. 30 (2019) 292–301.
[13] M. Obermayr, C. Vrettos, P. Eberhard, T. Däuwel, A discrete element model and its experimental validation for the prediction of draft forces in cohesive soil, J. Terramech. 53 (2014) 93–104, https://doi.org/10.1016/j.jterra.2014.04.003.
[14] L. Zhao, Y. Zhao, C. Bao, Q. Hou, A. Yu, Laboratory-scale validation of a DEM model of screening processes with circular vibration, Powder Technol. 303 (2016) 269–277.
[15] M. Ucgul, J.M. Fielke, C. Saunders, Three-dimensional discrete element modelling of tillage: Determination of a suitable contact model and parameters for a cohesionless soil, Biosyst. Eng. 121 (2014) 105–117, https://doi.org/10.1016/j.biosystemseng.2014.02.005.
[16] M.R. Fatahi, A. Farzanegan, DEM simulation of laboratory Knelson concentrator to study the effects of feed properties and operating parameters, Adv. Powder Technol. 28 (2017) 1443–1458.
[17] S. Schmelzle, S. Leppert, H. Nirschl, Influence of impeller geometry in a vertical mixer described by DEM simulation and the dispersion model, Adv. Powder Technol. 26 (2015) 1473–1482.
[18] H. Wei, Y. Zhao, J. Zhang, H. Saxén, Y. Yu, LIGGGHTS and EDEM application on charging system of ironmaking blast furnace, Adv. Powder Technol. 28 (2017) 2482–2487.
[19] A.P. Grima, T. Fraser, D.B. Hastie, P.W. Wypych, Discrete element modelling: trouble-shooting and optimisation tool for chute design (2011).
[20] D. Ilic, A. Roberts, C. Wheeler, Modelling bulk solid interactions in transfer chutes: accelerated flow, Chem. Eng. Sci. 209 (2019) 115197.
[21] D. Ilic, A. Roberts, C. Wheeler, A. Katterfeld, Modelling bulk solid flow interactions in transfer chutes: shearing flow, Powder Technol. 354 (2019) 30–44.
[22] D. Ilic, Development of design criteria for reducing wear in iron ore transfer chutes, Wear. 434 (2019) 202986.

[23] R. Cai, Y. Zhao, An experimentally validated coarse-grain DEM study of monodisperse granular mixing, Powder Technol. 361 (2020) 99–111.
[24] M.Z. Tekeste, T.R. Way, Z. Syed, R.L. Schafer, Modeling soil-bulldozer blade interaction using the discrete element method (DEM), J. Terramech. 88 (2020) 41–52.
[25] D. Kretz, S. Callau-Monje, M. Hitschler, A. Hien, M. Raedle, J. Hesser, Discrete element method (DEM) simulation and validation of a screw feeder system, Powder Technol. 287 (2016) 131–138.
[26] A. Edilbert, R. Spaargaren, C. Geijs, J. Ruijgrok, G. Lodewijks, D. Schott, Design of a High Speed Transfer Chute in a confined Space–A DEM Case Study, (n.d.).
[27] A.P. Grima, Quantifying and modelling mechanisms of flow in cohesionless and cohesive granular materials (2011).
[28] M. Ucgul, J.M. Fielke, C. Saunders, Defining the effect of sweep tillage tool cutting edge geometry on tillage forces using 3D discrete element modelling, Inform. Process. Agric. 2 (2015) 130–141, https://doi.org/10.1016/j.inpa.2015.07.001.
[29] J.B. Barr, J.M.A. Desbiolles, J.M. Fielke, M. Ucgul, Development and field evaluation of a high-speed no–till seeding system, Soil Tillage Res. 194 (2019) 104337.
[30] A.R. Cabral, R.A. Creaser, T. Nägler, B. Lehmann, A.R. Voegelin, B. Belyatsky, Trace-element and multi-isotope geochemistry of Late-Archean black shales in the Carajás iron-ore district, Brazil 362 (2013) 91–104, https://doi.org/10.1016/j.chemgeo.2013.08.041.
[31] Iron Ore Technical Working Group, Marine report (2013).
[32] British Standard Institution, BS EN1097-5: Determination of water content by drying in a ventilated oven, 2008.
[33] Iron Ore Technical Working Group, Reference tests (2013).
[34] M.C. Munro, A. Mohajerani, A review of the newly developed method used to prevent Liquefaction of iron ore fines on bulk carriers, Austral. Geomech. J. 51 (2016).
[35] P. ISO, ISO17828: 2016-Solid biofuels - Determination of bulk density, 2016.
[36] M. Kazhdan, H. Hoppe, Screened poisson surface reconstruction, ACM Trans. Graphics (ToG) 32 (2013) 1–13.
[37] S.W. Lommen, D.L. Schott, G. Lodewijks, Multibody dynamics model of a scissors grab for co-simulation with discrete element method, FME Trans. 40 (2012) 177–180.
[38] M.J. Mohajeri, R. Helmons, C. van Rhee, D.L. Schott, A hybrid particle-geometric scaling approach for elasto-plastic adhesive DEM contact models, Powder Technol. (2020).
[39] J.P. Morrissey, S.C. Thakur, J.Y. Ooi, EDEM Contact Model : Adhesive Elasto-Plastic Model (2014).
[40] S. Weisberg, Applied Linear Regression, John Wiley & Sons, 2005.